The Astronomical Journal, 163:195 (8pp), 2022 May https://doi.org/10.3847/1538-3881/ac5835

The Open Cluster Chemical Abundances and Mapping Survey. V. Chemical Abundances of CTIO/Hydra Clusters Using The Cannon

Amy E. Ray[1], Peter M. Frinchaboy[1], John Donor[1], S. D. Chojnowski[2], and Matthew Melendez[1]
[1] Department of Physics and Astronomy, Texas Christian University, TCU Box 298840 Fort Worth, TX 76129, USA; a.e.ray@tcu.edu, p.frinchaboy@tcu.edu, j.donor@tcu.edu, m.melendez@tcu.edu
[2] Department of Astronomy, New Mexico State University, Las Cruces, NM 88001, USA
Received 2021 August 5; revised 2022 January 28; accepted 2022 January 31; published 2022 April 5

Abstract

Open clusters are key chemical and age tracers of Milky Way evolution. While open clusters provide significant constraints on galaxy evolution, their use has been limited due to discrepancies in measuring abundances from different studies. We analyze medium-resolution ($R \sim 19{,}000$) Cerro Tololo Inter-American Observatory/Hydra spectra of giant stars in 58 open clusters using The Cannon to determine [Fe/H], [Mg/Fe], [Si/Fe], [Al/Fe], and [O/Fe]. This work adds an additional 55 primarily southern hemisphere open clusters calibrated to the Sloan Digital Sky Survey/Apache Point Observatory Galactic Evolution Experiment DR16 metallicity system. This uniform analysis is compared to previous studies [Fe/H] measurements for 23 clusters and we present spectroscopic metallicities for the first time for 35 open clusters.

Unified Astronomy Thesaurus concepts: Open star clusters (1160); Galactic abundances (2002); Milky Way evolution (1052); Chemical abundances (224)

Supporting material: machine-readable tables

1. Introduction

Open clusters provide reliable ages, a key constraint needed to study Galactic chemical evolution since their stars formed at the same time out of similar material. Many studies over the past few decades (e.g., Janes 1979; Yong et al. 2005; Bragaglia et al. 2008; Jacobson et al. 2009; Friel et al. 2010; Carrera & Pancino 2011; Magrini et al. 2017; Donor et al. 2018, 2020; Casamiquela et al. 2019) have used open clusters to explore the radial metallicity gradient in the Galactic disk, which has shown that clusters closer to the center are generally more metal-rich than clusters in the outer Galaxy.

However, there are several problems in using open clusters to study the Galactic abundance gradient. One is the number of open clusters used in individual studies. A way to improve the current knowledge in this area is to increase the number of clusters with known chemical abundances. There are roughly 2000 known open clusters (Cantat-Gaudin et al. 2020), but only a small portion of them have been analyzed chemically. Even the ones with measured abundance values can have substantial uncertainties from study to study (Yong et al. 2005). A few reasons for such large uncertainties are due to varying data quality, the type of data, and different data analysis methods between studies. Another source of uncertainty arises depending on which catalog each survey chose for the open cluster distances, as there are several that have determined substantially different distance results as discussed in Donor et al. (2018). This difference translates into widely varying results when attempting to determine a chemical abundance gradient across the disk of the Milky Way. Yong et al. (2012) and Donor et al. (2018, 2020) highlight this problem in their abundance gradient research. Netopil et al. (2016) compiled a homogenized sample of open cluster abundances, but there are still large uncertainties due to different types of observations and resolutions.

In this study, we put together a large uniform sample of open clusters observed with Cerro Tololo Inter-American Observatory (CTIO)/Hydra spectra. For this work we are using The Cannon, developed by Ness et al. (2015), which offers a unique way to find stellar parameters without having to use any models. Instead, this machine-learning method takes a subset of stars with known parameters or labels and creates a model based on pixel-to-pixel variations. This model can be applied to the rest of the set of stars to infer labels for them. Our training set is based on the Apache Point Observatory Galactic Evolution Experiment Data Release 16 (APOGEE DR16) system in order to correct the problems with current surveys that were listed above. This sample trained with stars from Donor et al. (2020; also on the APOGEE DR16 system) is designed to form a more extensive data set for Galactic abundance studies. The sections in this paper are as follows. Section 2 describes APOGEE DR16 and the observations taken for the sample of 58 open clusters. The Cannon and the training set that we used are described in Section 3. In Section 4, the results of this study are presented and we discuss comparisons to similar studies, and finally the conclusions are in Section 5.

2. Data and Observations

The primary data for this study comes from optical data near the calcium infrared triplet (7745–8730 Å) taken with the Hydra spectrograph using the CTIO 4 m telescope. Data was observed on UT 2002 March, 2003 March, 2003 July, and 2003 August. The data reduction and radial velocity and membership analysis of this data was conducted using IRAF[3]

[3] IRAF is distributed by the National Optical Astronomy Observatory, which is operated by the Association of Universities for Research in Astronomy, Inc., under cooperative agreement with the National Science Foundation.

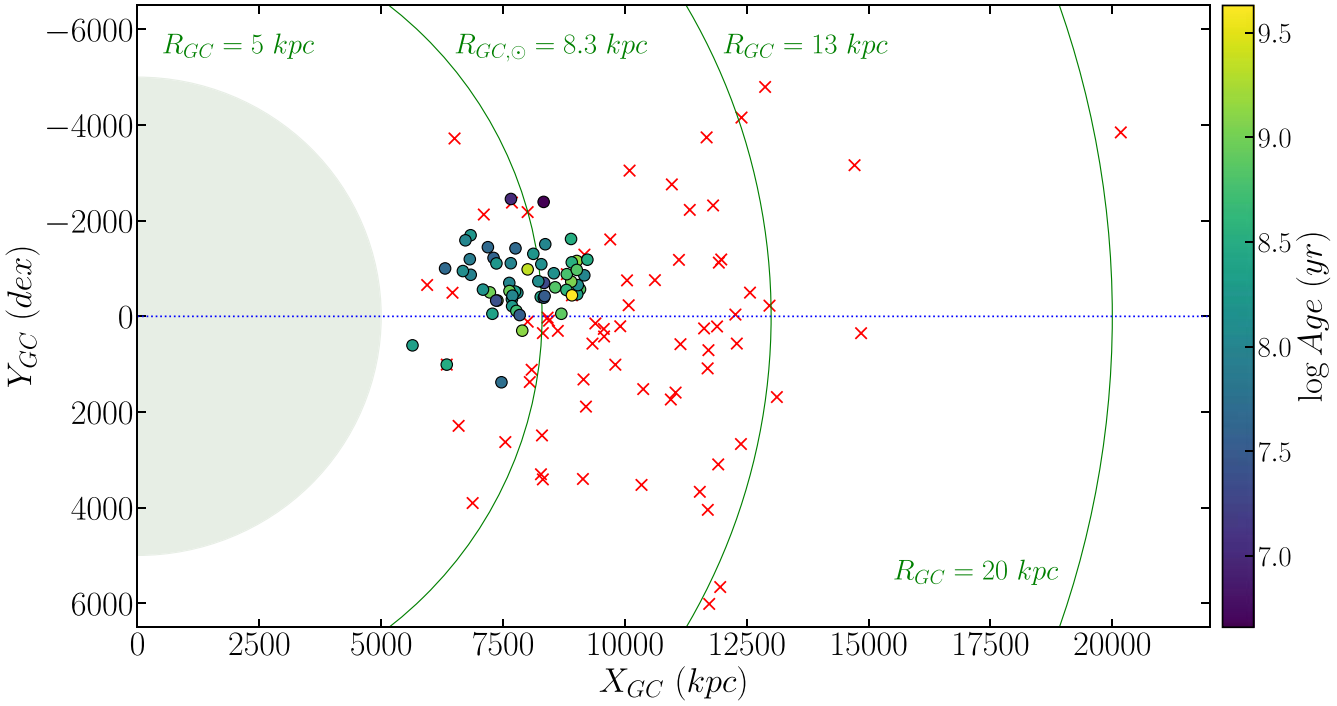

Figure 1. Spatial Galactic distribution of open clusters in this survey color coded with ages and R_{GC} distance from Cantat-Gaudin et al. (2020). Also shown are the locations of the OCCAM-IV DR16-based cluster from Donor et al. (2020) also updated with ages and R_{GC} distance from Cantat-Gaudin et al. (2020; red crosses).

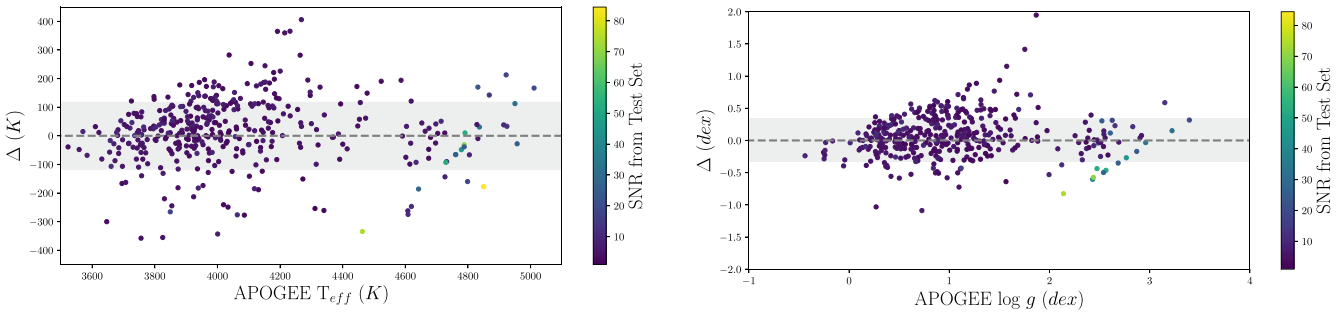

Figure 2. A comparison of effective temperature (T_{eff}) and surface gravity ($\log g$) values obtained by The Cannon and values obtained using APOGEE DR16 data. Most of the values fall within the scatter, which is illustrated by the gray shaded areas.

standard `ccdproc`, `dohydra`, and `fxcor` routines, which are fully described in Frinchaboy & Majewski (2008).

We have chosen to train The Cannon using data from the Sloan Digital Sky Survey's (SDSS; Eisenstein et al. 2011; Blanton et al. 2017) sixteenth data release (DR16; Holtzman et al. 2018; Ahumada et al. 2020; Jönsson et al. 2020) taken as part of APOGEE (APOGEE 2; Majewski et al. 2017). The APOGEE/DR16 data set includes about 430,000 stars, collected using two APOGEE spectrographs (Wilson et al. 2012) at Apache Point Observatory (APO; New Mexico Gunn et al. 2006) and Las Campanas Observatory (LCO; Chile Bowen & Vaughan 1973). For this study data from LCO provides a key overlap with our available training data. The APOGEE data reduction pipeline (Nidever et al. 2015; Holtzman et al. 2018) provides stellar atmospheric parameters and radial velocity measurements, while elemental abundances are provided from the APOGEE Stellar Parameter and Chemical Abundances Pipeline (ASPCAP; García Pérez et al. 2016; Holtzman et al. 2018; Jönsson et al. 2020).

For this study, we have applied The Cannon to derive chemical abundances for selected available elements, after applying a cut based on the radial velocity cross-correlation quality Tonry-Davis Ratio (TDR $\geqslant$ 11; Tonry & Davis 1979). After this cut we were able to use 25 stars from 3 clusters that are also observed with APOGEE DR16 in the training set. The Galactic distribution of the clusters in our sample are shown in Figure 1 using distances from Cantat-Gaudin et al. (2020) and also showing the positions of the high-quality clusters from Donor et al. (2020).

Additionally, to verify the results from Frinchaboy & Majewski (2008), we also used updated proper-motion data from Gaia DR2 (Gaia Collaboration et al. 2018) to recheck membership and found no change in membership between the Tycho-2 and Gaia-based proper-motion selection.

In addition to the data collected as part of Frinchaboy & Majewski (2008), observations of the the Sagittarius dwarf galaxy were also obtained on the same observing runs with the same instrument setup (Frinchaboy et al. 2012). Many of these

stars were also observed as part of the APOGEE survey and so these additional 365 spectra are included in The Cannon training set described below (TDR $\geqslant$ 11). Data reduction and membership is discussed fully in Frinchaboy et al. (2012), which is the same as described in Frinchaboy & Majewski (2008). The Cannon analysis of these Sagittarius data will be presented in P. M. Frinchaboy et al. (2022, in preparation).

3. The Cannon

3.1. Background

Many high-resolution abundance studies use the curve of growth, the Boltzmann and Saha equations, and stellar models to determine chemical abundances. However, for this medium-resolution, lower signal-to-noise ratio (S/N) data from CTIO Hydra, we have chosen to use The Cannon (Ness et al. 2015), which has been shown to work well for these types of data. The models, however, usually do not account for many distinctive factors in a star's atmosphere which means that research groups can get opposing values for the same star (Ness et al. 2015). For this study, the set of parameters used were $T_{\rm eff}$, $\log g$, [Fe/H], [Si/Fe], [Al/Fe], [Mg/Fe], and [O/Fe] following the methodology from Ho et al. (2017).

3.2. Training Set

The training set was comprised of 390 stars in total with 25 stars from open clusters and 365 from the Sagittarius dwarf galaxy. When this set was used to train The Cannon, a check was performed to determine if the output values were accurate. We first validated the output of the model by training The Cannon using 90% of the training sample, then deriving labels for the remaining 10%. We conducted this 10 times and analyzed how the input labels compared to the output labels from this cross-validation test.

Figure 2 illustrates the full training set one-to-one plots for $T_{\rm eff}$ and $\log g$, and Figure 3 shows similar plots for [Fe/H], [Si/Fe], [Al/Fe], [Mg/Fe], and [O/Fe]. Values obtained from The Cannon for the reference set are listed in Table 1 along with the values from APOGEE DR16. We find insignificant offset from DR16 for our parameters (Table 2), except maybe Si, but due to the lower S/N for training set stars in the study, we obtain less accurate parameters in comparison to some larger studies (e.g., Ho et al. 2017; Hasselquist et al. 2020). Due to the small offset, and large scatter, we find that the errors are dominated by the scatter from low S/Ns, which are significantly larger than the uncertainties from the APOGEE DR1 survey input labels.

4. Results & Discussion

Our resultant sample in this study consists of 58 open clusters with 237 member stars of which 35 have no previous spectroscopically determined metallicity measurements. The individual stellar abundance measurements for Fe as well as the α-elements magnesium, silicon, and oxygen, plus the odd-Z element aluminum, are presented in Table 3. The S/N for all cluster stars is computed at 8000 Å. We find that all of the elements scale relative to iron, in solar abundance ratios, as expected for clusters near the Sun and are within the normal of

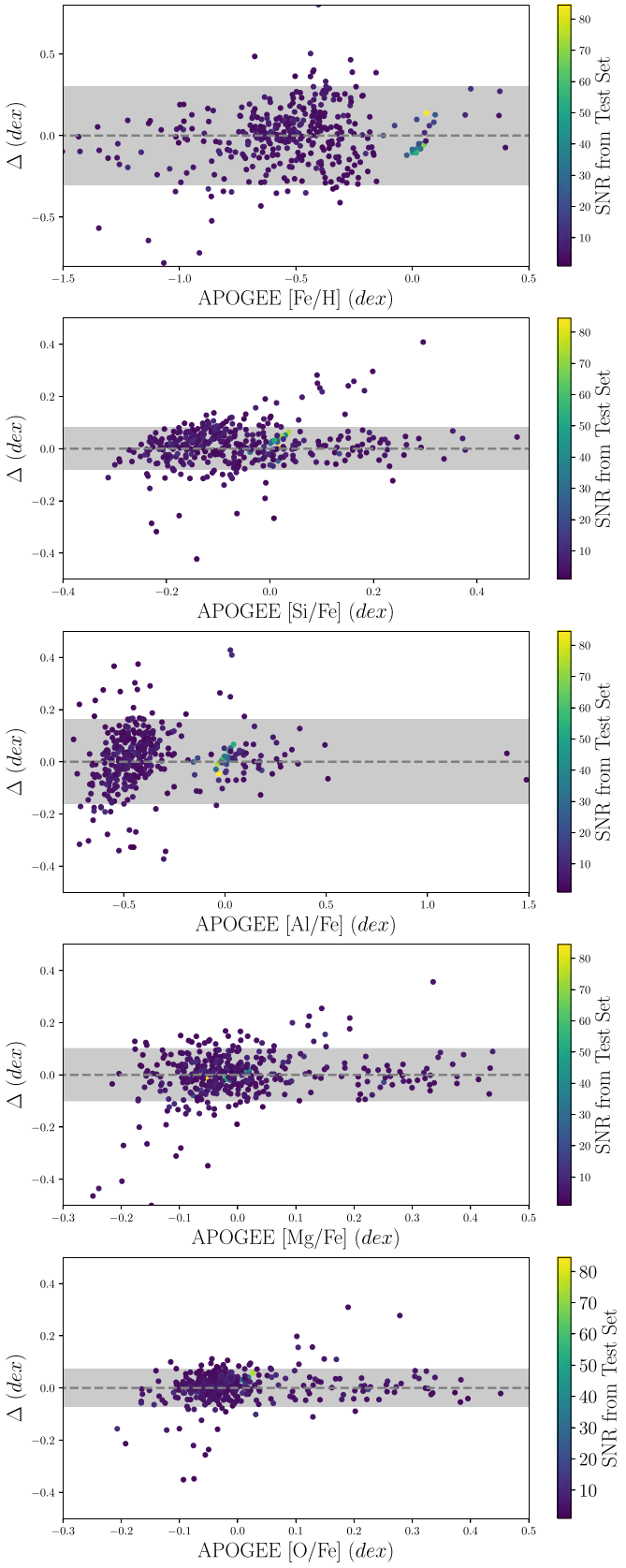

Figure 3. A comparison of [Fe/H], [Mg/Fe], [Si/Fe], [Al/Fe], and [O/Fe] values obtained by The Cannon and values obtained using APOGEE DR16 data. The shaded areas represent the acceptable scatter as in Figure 2.

Table 1
APOGEE DR16 Training Set Stars

2MASS ID	S/N (pixel^{-1})	Temp (K)	log g (dex)	[Fe/H] (dex)	[Si/Fe] (dex)	[Al/Fe] (dex)	[Mg/Fe] (dex)	[O/Fe] (dex)
2M18503032-2855221	9.2	3843	−0.4391	−0.8314	−0.2329	−0.5243	−0.1327	−0.1655
2M19040855-3103228	4.6	3523	−0.2544	−0.5450	−0.2667	−0.4611	−0.0940	−0.1646
2M18472966-2957462	7.7	3584	−0.2492	−0.5612	−0.1955	−0.3655	−0.0364	−0.0801
2M18554328-2937095	5.7	3558	−0.2422	−0.6150	−0.1624	−0.4713	+0.0011	−0.1635
2M18492810-2841275	9.0	3669	−0.2399	−0.6806	−0.1299	−0.5335	−0.0565	−0.0406
2M18514730-2857148	9.5	3570	−0.2336	−0.5483	−0.1026	−0.3219	−0.0369	−0.0277
2M18585375-3151470	7.3	3905	−0.1646	−0.7033	−0.1113	−0.4253	+0.0892	−0.0574
2M18470776-3017243	5.6	3685	−0.0545	−0.5985	−0.1252	−0.5417	+0.0497	−0.0252
2M18355640-2917489	5.8	3631	−0.0424	−0.7777	−0.1671	−0.4961	−0.0492	−0.0848
2M18575903-3203421	10.2	3678	+0.0109	−0.2958	−0.1947	−0.4098	−0.1184	−0.1434
			...					

Note. This table is available in its entirety in machine-readable form in the online journal. A portion is shown here for guidance regarding its form and content.
(This table is available in its entirety in machine-readable form.)

Table 2
APOGEE DR16/The Cannon Comparison for the Training Set

Parameter	Mean Offset	Std. Dev.
T_{eff}	+17 K	117 K
log g	+0.069 dex	0.32 dex
[Fe/H]	+0.001 dex	0.27 dex
[Si/Fe]	+0.010 dex	0.09 dex
[Al/Fe]	+0.004 dex	0.16 dex
[Mg/Fe]	−0.004 dex	0.10 dex
[O/Fe]	+0.004 dex	0.07 dex

solar neighborhood cluster mean abundances as seen in Donor et al. (2020). The resultant membership and cluster averages for all clusters studied are presented in Table 4, which are calculated as in Donor et al. (2020).

4.1. Direct Comparison to Donor et al. (2020)

To verify our results, we first compare to previous work using APOGEE DR16 directly (Donor et al. 2020). We have three clusters in common with some stars in the The Cannon training set. While with only a small subset of clusters, the studies agree within the uncertainties, as shown in Table 5.

4.2. Comparison to Other Surveys

The Santos et al. (2009) survey provided iron abundances for 13 open clusters using high-resolution spectra. There were eight clusters that overlapped with this survey, and their values are listed in Table 6. To better illustrate how the two surveys compare, we constructed a one-to-one plot of iron abundances from The Cannon versus values from three significant studies, including Santos et al. (2009), which is shown in Figure 4. All of the cluster values from Santos et al. (2009) lie within the average uncertainties, although our values were slightly more metal-poor.

The next comparison was to the Reddy et al. (2013) and Reddy et al. (2015) studies. Both examined a total of 12 clusters using high-resolution spectra. Here, there was also an overlap of seven clusters between this survey and the combined Reddy surveys. The values for each are shown in Table 6. These clusters are also shown on the one-to-one plot Figure 4. The values obtained by Reddy et al. (2013, 2015) were more

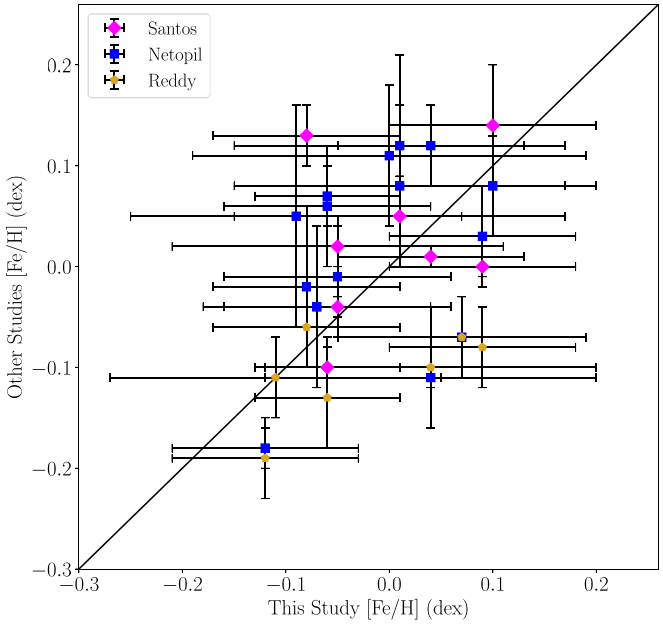

Figure 4. A comparison of the average [Fe/H] values in common open clusters from this survey and from the literature compilation in Table 6. Magenta clusters are from Santos et al. (2009), blue clusters are from Netopil et al. (2016), and orange clusters are from Reddy et al. (2013, 2015).

metal-poor than the values determined using The Cannon. The values of Reddy et al. (2013) and Reddy et al. (2015) have been found to be slightly more metal-poor with respect to most other high-resolution measurements, as summarized in Donor et al. (2018) and seen in Figure 2 from Reddy et al. (2016) in their comparison to previous literature results.

The last spectroscopic survey that we compared was by Netopil et al. (2016). They examined 172 clusters with a variety of data including low-, medium-, and high-resolution spectra as well as photometric data. The 12 clusters that overlapped had iron abundances determined from high-resolution spectra. All of the iron abundances are listed in Table 6 and the one-to-one plot Figure 4, which shows that the majority of the iron abundances are consistent, and that most clusters lie within the scatter range of The Cannon. There are two outliers which are discussed in Section 4.3.

Table 3
The Cannon Star Results for All Clusters

Cluster Name	2MASS ID	S/N (pixel^{-1})	Temp (K)	log g (dex)	[Fe/H] (dex)	[Si/Fe] (dex)	[Al/Fe] (dex)	[Mg/Fe] (dex)	[O/Fe] (dex)
Collinder 205	09001428-4901040	47.4	5174	3.45	−0.22	+0.22	+0.27	+0.20	+0.12
Collinder 205	09003203-4858199	28.0	4975	2.75	−0.45	+0.13	+0.21	+0.03	+0.16
Collinder 258	12271397-6043435	14.5	4896	2.59	−0.37	+0.09	+0.16	−0.03	+0.11
Collinder 258	12265230-6047561	20.1	5157	3.53	−0.17	+0.22	+0.28	+0.20	+0.12
Collinder 258	12291805-6031347	70.1	5213	3.88	−0.11	+0.29	+0.38	+0.25	+0.15
Harvard 10	16183313-5454573	47.6	4890	2.53	−0.30	+0.05	+0.12	+0.02	+0.09
Harvard 10	16183125-5457397	40.3	5138	3.28	−0.18	+0.21	+0.26	+0.19	+0.11
Harvard 10	16200896-5452364	21.3	4949	2.57	−0.44	+0.14	+0.25	+0.03	+0.14
Harvard 10	16195235-5503168	21.8	4933	2.68	−0.29	+0.05	+0.09	+0.02	+0.08
Harvard 10	16183216-5502259	44.9	5138	3.31	−0.18	+0.21	+0.25	+0.19	+0.11
			…						

Note. This table is available in its entirety in machine-readable form in the online journal. A portion is shown here for guidance regarding its form and content. (This table is available in its entirety in machine-readable form.)

Table 4
The Cannon-based Cluster Parameters

Cluster Name	Num Stars	log(*Age*)[a] (yrs)	[Fe/H] (dex)	[Si/Fe] (dex)	[Al/Fe] (dex)	[Mg/Fe] (dex)	[O/Fe] (dex)	New?
Collinder 205	2	6.66	−0.07 ± 0.19	+0.02 ± 0.06	+0.04 ± 0.11	−0.03 ± 0.07	+0.00 ± 0.05	Y
Collinder 258	2	7.99	−0.03 ± 0.19	+0.02 ± 0.06	+0.03 ± 0.11	−0.03 ± 0.07	+0.01 ± 0.05	Y
Harvard 10	4	8.30	−0.04 ± 0.14	+0.02 ± 0.05	+0.03 ± 0.08	−0.03 ± 0.05	+0.00 ± 0.04	N
IC 2395	1	7.31	+0.05 ± 0.27	+0.01 ± 0.09	+0.01 ± 0.16	+0.01 ± 0.10	+0.00 ± 0.07	N
IC 2488	3	8.21	+0.06 ± 0.16	+0.02 ± 0.05	+0.00 ± 0.09	−0.01 ± 0.06	+0.00 ± 0.04	N
IC 2581	1	7.01	−0.10 ± 0.27	−0.01 ± 0.09	+0.01 ± 0.16	−0.05 ± 0.10	−0.01 ± 0.07	N
IC 4651	9	9.22	+0.04 ± 0.09	+0.00 ± 0.03	+0.01 ± 0.05	+0.01 ± 0.03	+0.00 ± 0.02	N
IC 4756	3	9.11	−0.05 ± 0.16	+0.06 ± 0.05	−0.15 ± 0.09	+0.02 ± 0.06	+0.01 ± 0.04	N
Lynga 1	2	8.22	−0.01 ± 0.19	+0.01 ± 0.06	+0.02 ± 0.11	−0.04 ± 0.07	+0.00 ± 0.05	N
Lynga 2	3	8.01	+0.06 ± 0.16	+0.03 ± 0.05	+0.03 ± 0.09	+0.01 ± 0.06	+0.02 ± 0.04	N
NGC 1662	3	8.89	+0.04 ± 0.16	+0.06 ± 0.05	−0.07 ± 0.09	+0.05 ± 0.06	+0.04 ± 0.04	N
NGC 2215	7	8.84	−0.07 ± 0.10	+0.02 ± 0.03	+0.03 ± 0.06	−0.02 ± 0.04	+0.01 ± 0.03	N
NGC 2301	3	8.33	+0.09 ± 0.16	+0.01 ± 0.05	+0.02 ± 0.09	+0.01 ± 0.06	+0.01 ± 0.04	N
NGC 2323	3	8.12	+0.11 ± 0.16	+0.01 ± 0.05	+0.05 ± 0.09	+0.03 ± 0.06	+0.02 ± 0.04	N
NGC 2353	5	8.01	−0.16 ± 0.12	+0.03 ± 0.04	+0.04 ± 0.07	−0.03 ± 0.04	+0.02 ± 0.03	N
NGC 2354	10	9.15	−0.12 ± 0.09	+0.02 ± 0.03	+0.03 ± 0.05	−0.03 ± 0.03	+0.00 ± 0.02	N
NGC 2423	8	9.04	+0.10 ± 0.10	−0.01 ± 0.03	−0.01 ± 0.06	+0.00 ± 0.04	−0.02 ± 0.02	N
NGC 2437	3	8.48	−0.08 ± 0.16	+0.02 ± 0.05	+0.02 ± 0.09	−0.02 ± 0.06	−0.01 ± 0.04	Y
NGC 2447	17	8.76	−0.06 ± 0.07	+0.01 ± 0.02	+0.02 ± 0.04	−0.03 ± 0.02	−0.02 ± 0.02	T
NGC 2482	5	8.54	+0.07 ± 0.12	−0.01 ± 0.04	−0.01 ± 0.07	+0.01 ± 0.04	−0.01 ± 0.03	N
NGC 2516	3	8.38	−0.09 ± 0.16	+0.01 ± 0.05	+0.05 ± 0.09	−0.04 ± 0.06	−0.01 ± 0.04	N
NGC 2527	3	8.84	−0.11 ± 0.16	+0.02 ± 0.05	+0.03 ± 0.09	−0.04 ± 0.06	+0.00 ± 0.04	N
NGC 2539	9	8.84	−0.08 ± 0.09	+0.02 ± 0.03	+0.02 ± 0.05	−0.03 ± 0.03	−0.01 ± 0.02	N
NGC 2546	1	8.15	+0.06 ± 0.27	+0.01 ± 0.09	+0.04 ± 0.16	+0.04 ± 0.10	+0.02 ± 0.07	Y
NGC 2547	3	7.51	−0.05 ± 0.16	+0.02 ± 0.05	+0.03 ± 0.09	−0.02 ± 0.06	−0.01 ± 0.04	N
NGC 2548	3	8.59	+0.12 ± 0.16	−0.01 ± 0.05	+0.00 ± 0.09	+0.00 ± 0.06	−0.02 ± 0.04	N
NGC 2567	6	8.50	−0.07 ± 0.11	+0.01 ± 0.04	+0.02 ± 0.07	−0.03 ± 0.04	−0.01 ± 0.03	N
NGC 2579	2	…	−0.08 ± 0.19	+0.01 ± 0.06	+0.05 ± 0.11	−0.03 ± 0.07	−0.02 ± 0.05	Y
NGC 2669	1	8.13	−0.06 ± 0.27	+0.00 ± 0.09	+0.03 ± 0.16	−0.04 ± 0.10	−0.03 ± 0.07	Y
NGC 2670	2	8.01	−0.05 ± 0.19	+0.03 ± 0.06	+0.03 ± 0.11	−0.02 ± 0.07	+0.01 ± 0.05	N
NGC 2682	10	9.63	+0.09 ± 0.09	−0.02 ± 0.03	−0.01 ± 0.05	+0.00 ± 0.03	−0.02 ± 0.02	T
NGC 2925	1	8.11	+0.10 ± 0.27	+0.02 ± 0.09	+0.03 ± 0.16	+0.01 ± 0.10	+0.01 ± 0.07	N
NGC 3680	6	9.34	−0.05 ± 0.11	−0.01 ± 0.04	+0.01 ± 0.07	−0.03 ± 0.04	−0.02 ± 0.03	N
NGC 5138	2	7.68	−0.01 ± 0.19	+0.02 ± 0.06	+0.03 ± 0.11	−0.01 ± 0.07	+0.00 ± 0.05	N
NGC 5281	7	7.60	−0.02 ± 0.10	+0.01 ± 0.03	+0.02 ± 0.06	−0.04 ± 0.04	−0.01 ± 0.03	Y
NGC 5316	4	8.22	−0.01 ± 0.14	+0.01 ± 0.05	+0.03 ± 0.08	−0.03 ± 0.05	−0.02 ± 0.04	N
NGC 5460	2	8.20	−0.03 ± 0.19	+0.02 ± 0.06	+0.03 ± 0.11	−0.02 ± 0.07	−0.01 ± 0.05	N
NGC 5617	6	8.02	−0.04 ± 0.11	+0.02 ± 0.04	+0.03 ± 0.07	−0.03 ± 0.04	+0.00 ± 0.03	N
NGC 5662	2	8.30	+0.07 ± 0.19	+0.03 ± 0.06	+0.02 ± 0.11	+0.00 ± 0.07	+0.01 ± 0.05	N
NGC 5822	3	8.96	+0.01 ± 0.16	+0.01 ± 0.05	+0.02 ± 0.09	−0.03 ± 0.06	−0.02 ± 0.04	N

Table 4
(Continued)

Cluster Name	Num Stars	log(*Age*)[a] (yrs)	[Fe/H] (dex)	[Si/Fe] (dex)	[Al/Fe] (dex)	[Mg/Fe] (dex)	[O/Fe] (dex)	New?
NGC 5823	2	7.90	$+0.00 \pm 0.19$	$+0.02 \pm 0.06$	$+0.03 \pm 0.11$	-0.03 ± 0.07	-0.01 ± 0.05	N
NGC 6025	3	8.02	$+0.19 \pm 0.16$	$+0.01 \pm 0.05$	$+0.04 \pm 0.09$	$+0.02 \pm 0.06$	$+0.00 \pm 0.04$	N
NGC 6031	2	7.95	-0.07 ± 0.19	$+0.02 \pm 0.06$	$+0.03 \pm 0.11$	-0.03 ± 0.07	$+0.01 \pm 0.05$	N
NGC 6067	1	8.10	$+0.03 \pm 0.27$	$+0.03 \pm 0.09$	$+0.06 \pm 0.16$	-0.02 ± 0.10	$+0.02 \pm 0.07$	N
NGC 6124	19	8.28	$+0.07 \pm 0.06$	$+0.02 \pm 0.02$	$+0.02 \pm 0.04$	$+0.00 \pm 0.02$	$+0.01 \pm 0.02$	Y
NGC 6134	2	8.99	$+0.00 \pm 0.19$	$+0.01 \pm 0.06$	$+0.02 \pm 0.11$	-0.02 ± 0.07	$+0.00 \pm 0.05$	N
NGC 6167	3	8.19	$+0.05 \pm 0.16$	$+0.01 \pm 0.05$	$+0.02 \pm 0.09$	$+0.01 \pm 0.06$	$+0.01 \pm 0.04$	Y
NGC 6250	1	7.38	-0.15 ± 0.27	$+0.07 \pm 0.09$	-0.17 ± 0.16	$+0.03 \pm 0.10$	$+0.00 \pm 0.07$	Y
NGC 6281	7	8.71	-0.06 ± 0.10	$+0.02 \pm 0.03$	$+0.03 \pm 0.06$	-0.04 ± 0.04	$+0.00 \pm 0.03$	N
NGC 6405	6	7.54	-0.06 ± 0.11	$+0.02 \pm 0.04$	$+0.03 \pm 0.07$	-0.03 ± 0.04	$+0.01 \pm 0.03$	N
NGC 6416	6	8.36	-0.07 ± 0.11	$+0.02 \pm 0.04$	$+0.03 \pm 0.07$	-0.03 ± 0.04	$+0.01 \pm 0.03$	N
NGC 6603	1	8.34	$+0.05 \pm 0.27$	-0.01 ± 0.09	-0.01 ± 0.16	-0.04 ± 0.10	-0.01 ± 0.07	N
NGC 6705	3	8.49	$+0.01 \pm 0.16$	$+0.06 \pm 0.05$	-0.08 ± 0.09	$+0.01 \pm 0.06$	$+0.01 \pm 0.04$	T
NGC 6885	2	...	$+0.02 \pm 0.19$	$+0.06 \pm 0.06$	-0.08 ± 0.11	$+0.01 \pm 0.07$	$+0.01 \pm 0.05$	Y
Roslund 3	1	7.73	$+0.03 \pm 0.27$	$+0.01 \pm 0.09$	-0.06 ± 0.16	$+0.01 \pm 0.10$	$+0.00 \pm 0.07$	N
Ruprecht 119	2	7.68	$+0.08 \pm 0.19$	$+0.02 \pm 0.06$	$+0.03 \pm 0.11$	$+0.01 \pm 0.07$	$+0.01 \pm 0.05$	Y
Trumpler 10	2	7.51	-0.06 ± 0.19	$+0.02 \pm 0.06$	$+0.04 \pm 0.11$	-0.02 ± 0.07	$+0.00 \pm 0.05$	N
Trumpler 18	2	7.68	$+0.14 \pm 0.19$	$+0.01 \pm 0.06$	$+0.04 \pm 0.11$	$+0.03 \pm 0.07$	$+0.01 \pm 0.05$	N

Note.
[a] Cluster ages are taken from Cantat-Gaudin et al. (2020).

(This table is available in machine-readable form.)

Table 5
Average in Common Open Cluster Iron Abundance from Donor et al. (2020) Compared to (This Study)

	This Study		Donor	
Cluster Name	Number of Stars	[Fe/H] (dex)	Number of Stars	[Fe/H] (dex)
NGC 2447	17	-0.06 ± 0.07	3	-0.08 ± 0.01
NGC 2682	10	$+0.09 \pm 0.09$	32	$+0.01 \pm 0.03$
NGC 6705	3	$+0.01 \pm 0.16$	12	$+0.12 \pm 0.04$

The remaining clusters with iron abundances from smaller high-resolution studies were also examined for inconsistencies. Table 6 lists all of the values for [Fe/H] determined by The Cannon, the [Fe/H] values from the literature, and the type of data that was used. Most of the clusters fall within the range of scatter again (Table 6); however, three clusters did not. Reasons for why these values do not appear to agree are discussed in Section 4.3.

The cluster NGC 2682 is one of the most well-studied open clusters, therefore it was used as a calibration cluster. It also has an average [Fe/H] value determined from APOGEE DR16 data from Donor et al. (2020), making it a significant check on how well The Cannon produced values. The average [Fe/H] from Donor et al. (2020) was 0.01 ± 0.03, and this survey found a value of 0.09 ± 0.16. Additionally, the five other studies compared to in this paper with [Fe/H] determined for NGC 2682 (Pace et al. 2008; Santos et al. 2009; Reddy et al. 2013, 2015; Netopil et al. 2016) agree within the uncertainties.

4.3. Discrepancies

There were three clusters that were almost outside of the acceptable scatter when compared to the literature values, which are significant given our larger uncertainties due to the lower S/N of this study. This section discusses possible reasons why there were differences in iron abundance values.

The value obtained for NGC 6705 was within the uncertainty of Donor et al. (2020), however it was more metal-poor. This is likely due to Donor et al. (2020) having four times the number of member stars used for average abundance analysis as well as higher-resolution, higher-S/N spectra than this study. The same is also true when compared to the results of Netopil et al. (2016).

For NGC 1662, both Reddy et al. (2015) and Netopil et al. (2016) had values that were in agreement and for reference these values are listed in Tables 6 and 7. The value for NGC 1662 from this study was more metal-rich than both Reddy et al. (2015) and Netopil et al. (2016) and the comparison is shown in Figure 4. Each of these studies used high-resolution spectra of two stars where we used medium-resolution spectra of three stars.

The cluster NGC 2482 showed similar discrepancies to NGC 1662. Reddy et al. (2013) and Netopil et al. (2016) found more metal-poor values for this cluster and each only used one star for the average abundance analysis compared to the five stars used in this study, therefore the cluster membership of the other studies may be the reason for such a large offset. This comparison is also shown in Figure 4.

Table 6
Average Open Cluster Iron Abundance for Open Clusters in Common between This study and Other Literature Studies

Cluster Name	This Study Stars	This Study [Fe/H] (dex)	Other Studies Stars	Other Studies [Fe/H] (dex)	Citation
IC 2581	1	-0.10 ± 0.27	1	$-0.34 \pm \cdots$	Luck (1994)
IC 4651	9	$+0.04 \pm 0.09$	3	$+0.01 \pm 0.01$	Santos et al. (2009)
			18	$+0.12 \pm 0.04$	Netopil et al. (2016)
			5	$+0.12 \pm 0.05$	Pace et al. (2008).
			3	$+0.11 \pm 0.01$	Carretta et al. (2004)
IC 4756	3	-0.05 ± 0.16	3	$+0.02 \pm 0.02$	Santos et al. (2009)
			9	-0.02 ± 0.01	Bagdonas et al. (2018)
			12	-0.01 ± 0.10	Ting et al. (2012)
			2	$+0.01 \pm \cdots$	Pace et al. (2010)
NGC 1662	3	$+0.04 \pm 0.16$	2	-0.10 ± 0.06	Reddy et al. (2013, 2015)
			2	-0.11 ± 0.01	Netopil et al. (2016).
NGC 2354	10	-0.12 ± 0.09	2	-0.19 ± 0.04	Reddy et al. (2013, 2015)
			2	-0.18 ± 0.02	Netopil et al. (2016)
NGC 2423	8	$+0.10 \pm 0.10$	3	$+0.14 \pm 0.06$	Santos et al. (2009)
			3	$+0.08 \pm 0.05$	Netopil et al. (2016)
NGC 2447	17	-0.06 ± 0.07	3	-0.08 ± 0.01	Donor et al. (2020)
			3	-0.10 ± 0.03	Santos et al. (2009)
			3	-0.13 ± 0.05	Reddy et al. (2013, 2015)
			4	$+0.07 \pm 0.03$	Netopil et al. (2016)
			12	-0.17 ± 0.05	da Silveira et al. (2018)
NGC 2482	5	$+0.07 \pm 0.12$	1	-0.07 ± 0.04	Reddy et al. (2013, 2015)
			1	$-0.07 \pm \cdots$	Netopil et al. (2016)
NGC 2527	3	-0.11 ± 0.16	2	-0.11 ± 0.04	Reddy et al. (2013, 2015)
NGC 2516	3	-0.09 ± 0.16	2	$+0.05 \pm 0.11$	Netopil et al. (2016)
NGC 2539	9	-0.08 ± 0.09	3	$+0.13 \pm 0.03$	Santos et al. (2009)
			2	-0.06 ± 0.04	Reddy et al. (2013, 2015)
			4	-0.02 ± 0.08	Netopil et al. (2016)
			12	-0.03 ± 0.07	Martinez et al. (2020)
NGC 2548	3	$+0.12 \pm 0.16$	95	-0.06 ± 0.01	Sun et al. (2020)
NGC 2567	6	-0.07 ± 0.11	3	-0.04 ± 0.08	Netopil et al. (2016)
NGC 2682	10	$+0.09 \pm 0.09$	32	$+0.01 \pm 0.03$	Donor et al. (2020)
			3	$+0.00 \pm 0.01$	Santos et al. (2009)
			3	-0.08 ± 0.04	Reddy et al. (2013, 2015)
			27	$+0.03 \pm 0.05$	Netopil et al. (2016)
			6	$+0.03 \pm 0.04$	Pace et al. (2008)
NGC 3680	6	-0.05 ± 0.11	3	-0.04 ± 0.01	Santos et al. (2009)
			10	-0.01 ± 0.06	Netopil et al. (2016)
			6	-0.06 ± 0.07	Peña Suárez et al. (2018)
			11	-0.03 ± 0.02	Mitschang et al. (2012)
			2	$+0.04 \pm 0.03$	Pace et al. (2008)
NGC 5617	6	-0.04 ± 0.11	2	-0.18 ± 0.02	De Silva et al. (2015)
NGC 5822	3	$+0.01 \pm 0.16$	3	$+0.05 \pm 0.04$	Santos et al. (2009)
			7	$+0.08 \pm 0.08$	Netopil et al. (2016)
			11	-0.09 ± 0.06	Peña Suárez et al. (2018)
			3	$+0.15 \pm 0.08$	Pace et al. (2010)
			7	$+0.08 \pm 0.08$	Luck (1994)
NGC 6067	1	$+0.03 \pm 0.27$	5	$+0.19 \pm 0.05$	Alonso-Santiago et al. (2017)
NGC 6134	2	$+0.00 \pm 0.19$	8	$+0.11 \pm 0.07$	Netopil et al. (2016)
			6	$+0.15 \pm 0.07$	Carretta et al. (2004)
NGC 6281	7	-0.06 ± 0.10	2	$+0.06 \pm 0.06$	Netopil et al. (2016)
NGC 6405	6	-0.06 ± 0.11	44	$+0.07 \pm 0.03$	Kılıçoğlu et al. (2016)
NGC 6603	1	$+0.05 \pm 0.27$	7	$+0.34 \pm 0.15$	Carrera et al. (2015)
NGC 6705	3	$+0.01 \pm 0.16$	12	$+0.12 \pm 0.04$	Donor et al. (2020)
			21	$+0.12 \pm 0.09$	Netopil et al. (2016)

5. Conclusion

Using CTIO/Hydra medium-resolution ($R \sim 19{,}000$) spectroscopy of clusters stars with radial velocity and proper-motion membership determinations, we determined the mean [Fe/H] values for a set of 58 open clusters using The Cannon. With this study:

1. we measured the first spectroscopic metallicity [Fe/H] for 35 open clusters with member stars verified by Frinchaboy & Majewski (2008) and reverified with updated proper motions from Gaia Collaboration et al. (2018);

2. we confirm that the overall abundance scale, based on APOGEE DR16 (Ahumada et al. 2020), is generally consistent with other studies for the 22 clusters that have spectroscopic metallicity determinations; and
3. we find that the clusters in this study have abundance ratios for oxygen, silicon, magnesium, and aluminum consistent with solar values, which is reasonable for clusters near the solar neighborhood.

These clusters add to the work of Donor et al. (2020) yielding a combined data set of over 150 clusters, all on the APOGEE DR16 abundance scale.

We would like to thank Anna Ho for help in assisting in setting up The Cannon for this work. A.E.R., P.M.F., J.D., and M.M. acknowledge support for this research from the National Science Foundation (AST-1311835 and AST-1715662). P.M.F. also acknowledges that some of this was performed at the Aspen Center for Physics, which is supported by National Science Foundation grant PHY-1607611. P.M.F. also acknowledges travel support from NOAO/NOIRLab from the original collection of this data.

Funding for the Sloan Digital Sky Survey IV has been provided by the Alfred P. Sloan Foundation, the U.S. Department of Energy Office of Science, and the Participating Institutions. SDSS-IV acknowledges support and resources from the Center for High-Performance Computing at the University of Utah. The SDSS website is www.sdss.org.

SDSS-IV is managed by the Astrophysical Research Consortium for the Participating Institutions of the SDSS Collaboration including the Brazilian Participation Group, the Carnegie Institution for Science, Carnegie Mellon University, the Chilean Participation Group, the French Participation Group, Harvard-Smithsonian Center for Astrophysics, Instituto de Astrofísica de Canarias, The Johns Hopkins University, Kavli Institute for the Physics and Mathematics of the Universe (IPMU)/University of Tokyo, Lawrence Berkeley National Laboratory, Leibniz Institut für Astrophysik Potsdam (AIP), Max-Planck-Institut für Astronomie (MPIA Heidelberg), Max-Planck-Institut für Astrophysik (MPA Garching), Max-Planck-Institut für Extraterrestrische Physik (MPE), National Astronomical Observatories of China, New Mexico State University, New York University, University of Notre Dame, Observatário Nacional/MCTI, The Ohio State University, Pennsylvania State University, Shanghai Astronomical Observatory, United Kingdom Participation Group, Universidad Nacional Autónoma de México, University of Arizona, University of Colorado Boulder, University of Oxford, University of Portsmouth, University of Utah, University of Virginia, University of Washington, University of Wisconsin, Vanderbilt University, and Yale University.

This work has made use of data from the European Space Agency (ESA) mission Gaia (https://www.cosmos.esa.int/gaia), processed by the Gaia Data Processing and Analysis Consortium (DPAC, https://www.cosmos.esa.int/web/gaia/dpac/consortium). Funding for the DPAC has been provided by national institutions, in particular the institutions participating in the Gaia Multilateral Agreement.

This research made use of Astropy, a community-developed core Python package for Astronomy (Astropy Collaboration et al. 2013, 2018).

Facilities: Sloan (APOGEE), FLWO:2MASS, Gaia, CTIO: Hydra.

Software: Astropy (Astropy Collaboration et al. 2013, 2018), The Cannon (Ness et al. 2015; Ho et al. 2017).

ORCID iDs

Peter M. Frinchaboy https://orcid.org/0000-0002-0740-8346
S. D. Chojnowski https://orcid.org/0000-0001-9984-0891

References

Ahumada, R., Prieto, C. A., Almeida, A., et al. 2020, ApJS, 249, 3
Alonso-Santiago, J., Negueruela, I., Marco, A., et al. 2017, MNRAS, 469, 1330
Astropy Collaboration, Price-Whelan, A. M., Sipőcz, B. M., et al. 2018, AJ, 156, 123
Astropy Collaboration, Robitaille, T. P., Tollerud, E. J., et al. 2013, A&A, 558, A33
Bagdonas, V., Drazdauskas, A., Tautvaišienė, G., Smiljanic, R., & Chorniy, Y. 2018, A&A, 615, A165
Blanton, M. R., Bershady, M. A., Abolfathi, B., et al. 2017, AJ, 154, 28
Bowen, I. S., & Vaughan, A. H. J. 1973, ApOpt, 12, 1430
Bragaglia, A., Sestito, P., Villanova, S., et al. 2008, A&A, 480, 79
Cantat-Gaudin, T., Anders, F., Castro-Ginard, A., et al. 2020, A&A, 640, A1
Carrera, R., Casamiquela, L., Ospina, N., et al. 2015, A&A, 578, A27
Carrera, R., & Pancino, E. 2011, A&A, 535, A30
Carretta, E., Bragaglia, A., Gratton, R. G., & Tosi, M. 2004, A&A, 422, 951
Casamiquela, L., Blanco-Cuaresma, S., Carrera, R., et al. 2019, MNRAS, 490, 1821
da Silveira, M. D., Pereira, C. B., & Drake, N. A. 2018, MNRAS, 476, 4907
De Silva, G. M., Carraro, G., D'Orazi, V., et al. 2015, MNRAS, 453, 106
Donor, J., Frinchaboy, P. M., Cunha, K., et al. 2018, AJ, 156, 142
Donor, J., Frinchaboy, P. M., Cunha, K., et al. 2020, AJ, 159, 199
Eisenstein, D. J., Weinberg, D. H., Agol, E., et al. 2011, AJ, 142, 72
Friel, E. D., Jacobson, H. R., & Pilachowski, C. A. 2010, AJ, 139, 1942
Frinchaboy, P. M., & Majewski, S. R. 2008, AJ, 136, 118
Frinchaboy, P. M., Majewski, S. R., Muñoz, R. R., et al. 2012, ApJ, 756, 74
Gaia Collaboration, Brown, A. G. A., Vallenari, A., et al. 2018, A&A, 616, A1
García Pérez, A. E., Allende Prieto, C., Holtzman, J. A., et al. 2016, AJ, 151, 144
Gunn, J. E., Siegmund, W. A., Mannery, E. J., et al. 2006, AJ, 131, 2332
Hasselquist, S., Zasowski, G., Feuillet, D. K., et al. 2020, ApJ, 901, 109
Ho, A. Y. Q., Ness, M. K., Hogg, D. W., et al. 2017, ApJ, 836, 5
Holtzman, J. A., Hasselquist, S., Shetrone, M., et al. 2018, AJ, 156, 125
Jacobson, H. R., Friel, E. D., & Pilachowski, C. A. 2009, AJ, 137, 4753
Janes, K. A. 1979, ApJS, 39, 135
Jönsson, H., Holtzman, J. A., Allende Prieto, C., et al. 2020, AJ, 160, 120
Kılıçoğlu, T., Monier, R., Richer, J., Fossati, L., & Albayrak, B. 2016, AJ, 151, 49
Luck, R. E. 1994, ApJS, 91, 309
Magrini, L., Randich, S., Kordopatis, G., et al. 2017, A&A, 603, A2
Majewski, S. R., Schiavon, R. P., Frinchaboy, P. M., et al. 2017, AJ, 154, 94
Martinez, C. F., Holanda, N., Pereira, C. B., & Drake, N. A. 2020, MNRAS, 494, 1470
Mitschang, A. W., De Silva, G. M., & Zucker, D. B. 2012, MNRAS, 422, 3527
Ness, M., Hogg, D. W., Rix, H.-W., Ho, A. Y. Q., & Zasowski, G. 2015, ApJ, 808, 16
Netopil, M., Paunzen, E., Heiter, U., & Soubiran, C. 2016, A&A, 585, A150
Nidever, D. L., Holtzman, J. A., Allende Prieto, C., et al. 2015, AJ, 150, 173
Pace, G., Danziger, J., Carraro, G., et al. 2010, A&A, 515, A28
Pace, G., Pasquini, L., & François, P. 2008, A&A, 489, 403
Peña Suárez, V. J., Sales Silva, J. V., Katime Santrich, O. J., Drake, N. A., & Pereira, C. B. 2018, ApJ, 854, 184
Reddy, A. B. S., Giridhar, S., & Lambert, D. L. 2013, MNRAS, 431, 3338
Reddy, A. B. S., Giridhar, S., & Lambert, D. L. 2015, MNRAS, 450, 4301
Reddy, A. B. S., Lambert, D. L., & Giridhar, S. 2016, MNRAS, 463, 4366
Santos, N. C., Lovis, C., Pace, G., Melendez, J., & Naef, D. 2009, A&A, 493, 309
Sun, Q., Deliyannis, C. P., Steinhauer, A., Twarog, B. A., & Anthony-Twarog, B. J. 2020, AJ, 159, 220
Ting, Y.-S., De Silva, G. M., Freeman, K. C., & Parker, S. J. 2012, MNRAS, 427, 882
Tonry, J., & Davis, M. 1979, AJ, 84, 1511
Wilson, J. C., Hearty, F., Skrutskie, M. F., et al. 2012, Proc. SPIE, 8446, 84460H
Yong, D., Carney, B. W., & Friel, E. D. 2012, AJ, 144, 95
Yong, D., Carney, B. W., & Teixera de Almeida, M. L. 2005, AJ, 130, 597